

# PHOTONICS Research

## Widely tunable continuous-wave visible and mid-infrared light generation based on a dual-wavelength switchable and tunable random Raman fiber laser

HAN WU,<sup>1,†</sup> WEIZHE WANG,<sup>1,†</sup> BO HU,<sup>1</sup> YANG LI,<sup>1</sup> KAN TIAN,<sup>1</sup> RUI MA,<sup>2</sup> CHUNXIAO LI,<sup>3</sup> JUN LIU,<sup>2,4</sup> JIYONG YAO,<sup>3,5</sup> AND HOUKUN LIANG<sup>1,6</sup>

<sup>1</sup>College of Electronics and Information Engineering, Sichuan University, Chengdu 610064, China

<sup>2</sup>International Collaborative Laboratory of 2D Materials for Optoelectronics Science and Technology of Ministry of Education, Institute of Microscale Optoelectronics, Shenzhen University, Shenzhen 518060, China

<sup>3</sup>Beijing Center for Crystal Research and Development, Key Laboratory of Functional Crystals and Laser Technology, Technical Institute of Physics and Chemistry, Chinese Academy of Sciences, Beijing 100190, China

<sup>4</sup>e-mail: liu-jun-1987@live.cn

<sup>5</sup>e-mail: jyao@mail.ipc.ac.cn

<sup>6</sup>e-mail: hkliang@scu.edu.cn

<sup>†</sup>These authors contributed equally to this paper.

Received 17 January 2023; revised 8 March 2023; accepted 11 March 2023; posted 20 March 2023 (Doc. ID 485813); published 1 May 2023

Nonlinear frequency conversion of wavelength agile and high-power random fiber lasers can provide a promising way to generate continuous-wave (CW) visible and mid-infrared (MIR) light with unique properties such as the continuous modeless spectrum, low temporal/spatial coherence, and high temporal stability. Here, we report a dual-wavelength switchable and tunable random Raman fiber laser (RRFL) based on a phosphosilicate fiber that has two Raman gain peaks for the first time and demonstrate its superior capability to generate widely tunable CW visible and mid-infrared light via nonlinear frequency conversions. By using the combination of a tunable pump and two tunable gratings in Littrow configuration that can provide separated point feedback for the two Stokes wavelengths corresponding to silica- and phosphorus-related Raman peaks, the spectrum of an RRFL can be flexibly manipulated for the aim of nonlinear frequency conversions, including single-wavelength tunable emission at the 1.1  $\mu\text{m}$  or 1.2  $\mu\text{m}$  band for second-harmonic generation (SHG), dual-wavelength simultaneously tunable emission at the 1.1  $\mu\text{m}$  and 1.2  $\mu\text{m}$  bands for the sum-frequency generation (SFG), and dual-wavelength separation tunable emission for difference-frequency generation (DFG). As a result, with the combination of SHG and SFG in a periodically poled lithium niobate crystal array, we experimentally demonstrate the broadest tuning range (560–630 nm) of visible light generated from an RRFL, to the best of our knowledge. The tunable MIR light in the range of 10.7–12.3  $\mu\text{m}$  is also demonstrated through DFG of an RRFL operating in separation tunable dual-wavelength emission mode in a BaGa<sub>4</sub>Se<sub>7</sub> (BGSe) crystal, which is the first realization of >10  $\mu\text{m}$  CW DFG in the BGSe crystal. We believe the developed dual-wavelength switchable and tunable RRFL can provide a new compact, robust, and cost-effective platform to realize broadly tunable light in both the visible and MIR regions, which can also find potential applications in imaging, sensing, and temporal ghost imaging in various spectral bands. © 2023 Chinese Laser Press

<https://doi.org/10.1364/PRJ.485813>

### 1. INTRODUCTION

Random fiber lasers (RFLs) based on random Rayleigh scattering feedback in passive fiber have attracted a great deal of attention in recent years and have been demonstrated as new platforms for the generation of high-performance fiber lasing with unique features [1–3]. Particularly, a random Raman fiber laser (RRFL) with short cavity length can generate random

lasing with an ultrahigh efficiency approaching quantum limits [4,5], which provides a new route for high-power laser especially in the wavelength bands that are outside of the emission spectral regions of rare-earth-doped fiber lasers. Until now, the maximum output power of an RRFL has reached the kilowatt level [6]. Moreover, due to the special power distribution characteristics of an RRFL, the realization of spectral manipulation

of a high-power RRFL is feasible through adopting low-power spectral tuning devices [7,8]. Hence, the tunable RRFL with flat tuning curve and power-equalized multiwavelength generation can be realized [9–11]. Taking advantage of cascaded stimulated Raman scattering and simple cavity configuration without the necessity of a series of fiber Bragg grating pairs, an RRFL can lase at arbitrary wavelengths across the fiber transparency window [12–15], and tunable cascaded RRFLs covering the 1.1–2  $\mu\text{m}$  region have been realized [12–15]. Moreover, with the feature of modeless spectrum free of mode competition, RFLs have been verified experimentally to have better temporal intensity stability than conventional fiber lasers [16,17]. The modeless spectrum can also lead to the random temporal intensity fluctuations of RFLs [18,19], making them excellent candidates for correlation-based applications such as temporal ghost imaging [18] and random bit generation [19–21]. The spatial mode of an RFL can also be manipulated [22–24] and the low spatial coherence RFLs have important applications in speckle-free imaging [22] and speckle-correlated imaging [25].

With the ability of wavelength-agile and high-power fiber lasing generation, RFLs can be used to realize continuous-wave (CW) visible and mid-infrared (MIR) lasing via nonlinear frequency conversions. Through the single-pass nonlinear frequency conversion process, the generated visible or MIR light can inherit the unique properties of RFLs, such as continuous modeless spectrum, low temporal/spatial coherence, and high temporal stability. Therefore, the output visible or MIR lasing can be used for particular applications such as speckle-free imaging, speckle-correlated imaging, temporal ghost imaging, and chaotic lidar [26]. For visible light generation, second-harmonic generation (SHG) of an RRFL and an ytterbium-doped RFL has been reported to generate watt-level visible light at fixed wavelengths [27–29]. The amplified spectrum-filtered RFL with tailored statistics properties was used to further enhance the efficiency of SHG [30]. The SHG of a tunable ytterbium-doped RFL was reported to realize tunable green light with a limited tuning range from 529.9 to 537.3 nm [30]. Very recently, SHG and sum-frequency generation (SFG) of a 1120/1238 nm dual-wavelength switchable RRFL have been reported to generate switchable output of green, yellow, and red light at fixed wavelengths of 560, 588, and 619 nm, respectively [31]. However, until now, broadly tunable visible light covering various colors generated from an RFL still remains underdeveloped. As for the MIR light generation from an RFL, the difference-frequency generation (DFG) of a tunable cascaded RRFL and a tunable ytterbium-doped RFL in a periodically poled lithium niobate (PPLN) crystal was reported to generate 2.9–4.4  $\mu\text{m}$  tunable MIR light, which breaks the tuning range limitation by using the DFG from conventional ytterbium-doped and erbium-doped fiber lasers [32]. Moreover, to realize long-wavelength MIR light, a new promising nonlinear crystal  $\text{BaGa}_4\text{Se}_7$  (BGSe) featuring a broad transparency range spanning from 0.47 to 18  $\mu\text{m}$ , decent nonlinearity, and relatively high damage threshold [33,34] has been employed for performing DFG of a cascaded RRFL and a tunable ytterbium-doped RFL. MIR radiation with the tuning wavelengths ranging from 5.5 to 9.5  $\mu\text{m}$  has been

experimentally realized [35]. However, in these demonstrations, two different types of RFLs are required in the DFG process and there has been no report of DFG of a dual-wavelength RFL yet. In addition, the ability to generate >10  $\mu\text{m}$  CW DFG with BGSe crystal still remains unexplored [35,36].

In this paper, we develop a dual-wavelength switchable and tunable RRFL based on a phosphosilicate fiber for the first time. The spectrum of the proposed RRFL can be flexibly manipulated to meet the requirements of different nonlinear frequency conversion processes, including single-wavelength tunable emission at the 1.1  $\mu\text{m}$  or 1.2  $\mu\text{m}$  band for SHG, dual-wavelength simultaneously tunable emission in the 1.1  $\mu\text{m}$  and 1.2  $\mu\text{m}$  spectral regions for SFG, and separation tunable dual-wavelength emission for DFG. Tunable CW visible lasing with a record tuning range (560–630 nm) generated from an RFL is realized via SHG and SFG employing the proposed RRFL in a PPLN crystal and 10.7–12.3  $\mu\text{m}$  tunable CW MIR radiation is experimentally demonstrated through DFG of the proposed RRFL in a BGSe crystal. The experimental results reveal that the proposed dual-wavelength switchable and tunable RRFL can provide an excellent platform for performing multifunctional nonlinear frequency conversion processes and generating widely tunable light in both the visible and MIR regions.

## 2. SETUP AND CHARACTERIZATION OF DUAL-WAVELENGTH SWITCHABLE AND TUNABLE RRFL

The experimental setup for the dual-wavelength switchable and tunable RRFL is shown in Fig. 1(a). The RRFL consists of a wavelength tunable pump source, a 1-km-long phosphosilicate fiber (FORC-Photonics PDF-5/125) to provide both Raman gain and random Rayleigh scattering feedback, and a point feedback unit consisting of two gratings in Littrow configuration to form the forward-pumped half-open cavity for the RRFL. The fiber length is roughly optimized for enhancing output lasing power with the available pump power. The Raman gain spectrum of the used phosphosilicate fiber is shown in Fig. 1(b); the existence of the silica- and phosphorus-related Raman peaks makes it possible to generate dual-wavelength random lasing [31,37]. The wavelength tunable pump source is a home-made ytterbium-doped RFL that can generate continuously tunable lasing from 1045 to 1095 nm; more details can be found in Ref. [35]. A wavelength-division multiplexer (WDM, pass port: 1040–1095 nm; reflection port: 1100–1700 nm) is used to inject the tunable pump into the phosphosilicate fiber and extract the Stokes light to the point feedback unit. The insertion loss of the WDM is 0.6 dB. The splicing loss between the WDM and phosphosilicate fiber is about 0.6 dB. In the point feedback unit, the Stokes light is first collimated by using a fiber collimator and then is divided into two paths after a beam splitter (1000–1300 nm AR-coated). Two gratings (600 lines/mm) in the Littrow configuration are used to separately provide wavelength-selective feedback for the Stokes light corresponding to the silica- and phosphorus-related Raman peaks, respectively. The reflectivity of the grating is about 55%. By rotating the angles of two gratings, their reflection wavelengths of two gratings can be

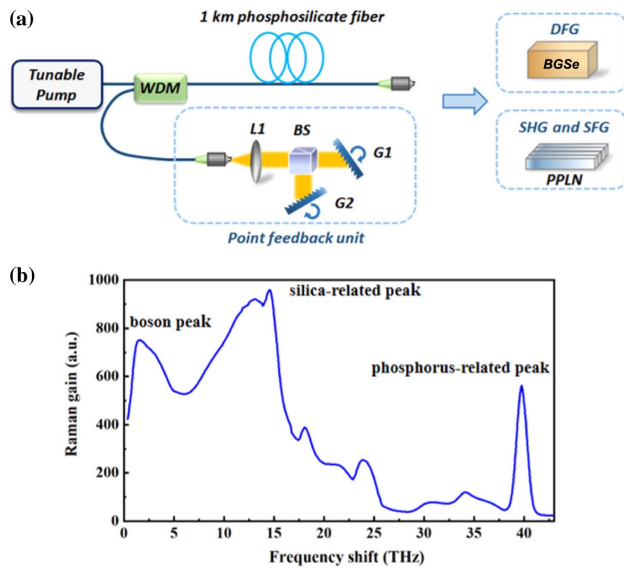


**Fig. 1.** (a) Experimental setup for the dual-wavelength switchable and tunable RRFL. G, grating; WDM, wavelength-division multiplexer; BS, 1:1 beam splitter; L, lens. (b) Raman gain spectrum of the used phosphosilicate fiber.

tuned individually. With the combination of a tunable pump and a specially designed point feedback unit, it is flexible to select the random lasing wavelength corresponding to the silica-related Raman peak and/or the phosphorus-related one together with a certain tuning range. It should be noted that since the two gratings can only provide point feedback for the first-order random Raman fiber lasing, the second-order random lasing is generated in a completely open cavity configuration and has a relatively high threshold, which is beneficial for power scaling of first-order random Raman fiber lasing. All the fiber ends are angle cleaved to suppress the unwanted backward reflection. The output of the RRFL is at the end of the fiber and is characterized by an optical spectrum analyzer (Yokogawa AQ6370D) and a power meter (Ophir 30A-BB-18). The generated dual-wavelength switchable and tunable random fiber lasing can be used for SHG and SFG in the PPLN crystal or DFG in the BGSe nonlinear crystal.

### A. Single-Wavelength Tunable Emission for SHG

For the purpose of efficient SHG, single-wavelength tunable lasing is required. For the proposed RRFL, it is possible to realize single-wavelength tunable emission at either the 1.1  $\mu\text{m}$  band or the 1.2  $\mu\text{m}$  band.

To generate single-wavelength emission at the 1.1  $\mu\text{m}$  band, at the fixed pump wavelength, the reflection wavelength of grating 1 (G1) in the point feedback unit is set to match the frequency shift of the silica-related Raman peak (13.2 THz), while the reflection wavelength of grating 2 (G2) is outside the gain spectrum of the phosphorus-related Raman peak (39.9 THz). In this way, only the random lasing at the silica-related Raman peak can be stimulated. Furthermore, by simultaneously tuning the pump wavelength and the matched reflection wavelength of G1, single-wavelength tunable random lasing at the 1.1  $\mu\text{m}$  band can be realized. The spectra of single-wavelength tunable

random lasing at the 1.1  $\mu\text{m}$  band are plotted in Fig. 2(a). It can be seen that the single-wavelength lasing line at 1.1  $\mu\text{m}$  dominates the spectrum and the wavelength tuning range is from 1105 to 1160 nm. At the maximum pump power of 18 W (the launched pump power into phosphosilicate fiber is 13.6 W), the output powers of the 1.1  $\mu\text{m}$  single-wavelength tunable RRFL at different center wavelengths are shown in Fig. 2(b). The output powers fluctuate around 6.5 W and are in the range of 6.1–7.3 W across the whole wavelength tuning range. There is no sign of generating second-order random lasing; therefore, further power scaling is feasible with a more

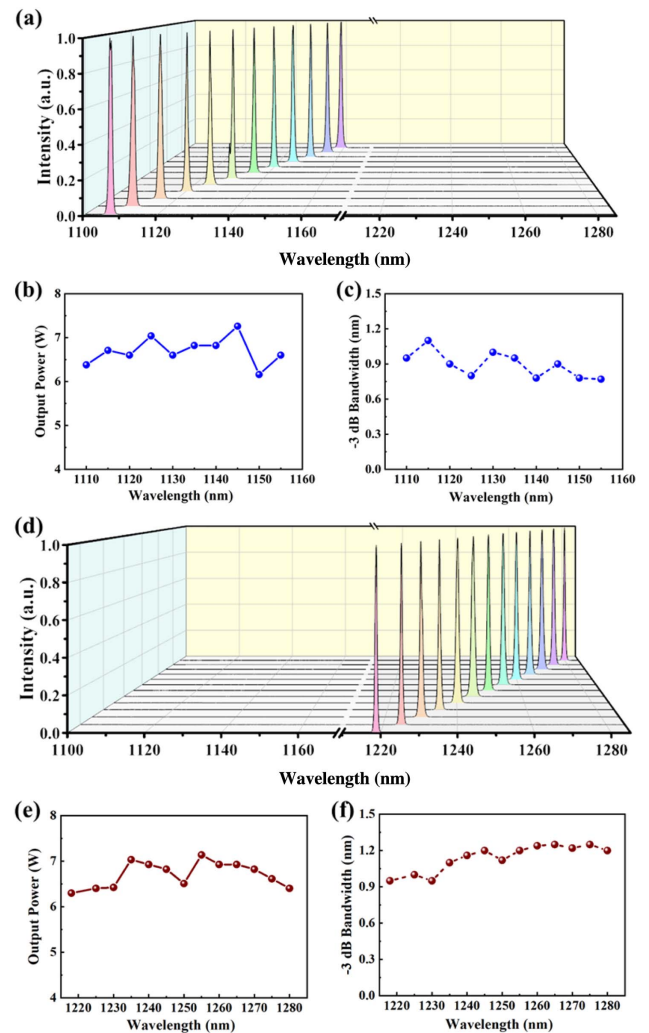


**Fig. 2.** (a) Spectra of the wavelength tunable RRFL based on the silica-related Raman peak with a wavelength tuning range from 1105 to 1160 nm. (b) Output powers of the wavelength tunable RRFL based on the silica-related Raman peak as a function of center wavelengths. (c)  $-3$  dB bandwidths of the wavelength tunable RRFL based on the silica-related Raman peak as a function of center wavelengths. (d) Spectra of the wavelength tunable RRFL based on the phosphorus-related Raman peak with a wavelength tuning range from 1217 to 1280 nm. (e) Output powers of the wavelength tunable RRFL based on the phosphorus-related Raman peak as a function of center wavelengths. (f)  $-3$  dB bandwidths of wavelength tunable RRFL based on the phosphorus-related Raman peak as a function of center wavelengths.

powerful pump. Meanwhile, the  $-3$  dB bandwidths of single-wavelength tunable  $1.1 \mu\text{m}$  random lasing at maximum output powers are also recorded in Fig. 2(c). The  $-3$  dB bandwidths fluctuate around  $0.9$  nm and are in the range of  $0.75$ – $1.15$  nm. Since the lasing bandwidth plays an important role in SHG efficiency, further efforts can be done to reduce the bandwidth of RRFL by using the volume Bragg grating with a much narrower reflection bandwidth [38] or the etalon assisted point reflector [39] in the point feedback unit instead of the diffraction gratings used in our current setup. It should be noted that the spectrum of random fiber lasing experiences greater broadening in a forward-pumped structure compared to a backward-pumped one [29,40]; therefore, using a backward-pumped RRFL could result in narrower random lasing emission for more efficient SHG [29]. However, in the backward-pumped RRFL, pulsing operation can be realized due to the spatiotemporal gain modulation [41]. Therefore, in order to realize quasi-CW operation of the RRFL [31], we use a forward-pumped structure in this work.

Similarly, if the reflection wavelength of G2 matches the given pump wavelength and the frequency shift of the phosphorus-related peak, and the reflection wavelength of G1 is outside the gain spectrum of the silica-related Raman peak, the single-wavelength random lasing emission at the  $1.2 \mu\text{m}$  band can be realized. By simultaneously tuning the pump wavelength and rotating the angle of G2 to change the reflection wavelength, single-wavelength tunable random lasing emission in the range of  $1217$ – $1280$  nm can be experimentally demonstrated, as depicted in Fig. 2(d). The output powers at the maximum pump power of  $18$  W and  $-3$  dB bandwidths at the maximum output power of the tunable  $1.2 \mu\text{m}$  RRFL as a function of center wavelengths are shown in Fig. 2(e) and Fig. 2(f), respectively. The maximum output powers range from  $6.3$  W to  $7.2$  W and the  $-3$  dB bandwidths are in the range of  $0.9$ – $1.25$  nm of  $1.2 \mu\text{m}$  single-wavelength lasing lines.

### B. Dual-Wavelength Simultaneously Tunable Emission for SFG

For the aim of generating tunable visible light via SFG, a dual-wavelength simultaneously tunable operation mode is preferred. In the proposed RRFL, when the pump wavelength is tuned, if we simultaneously change the reflection wavelengths of G1 and G2 to match the frequency shift of the silica-related peak and phosphorus-related peak, respectively, dual-wavelength random lasing at the  $1.1 \mu\text{m}$  and  $1.2 \mu\text{m}$  bands can be stimulated and their wavelengths can be simultaneously tuned along with the pump wavelength tuning. To maximize the SFG efficiency, the dual-wavelength RRFL should have an equal power ratio of the two laser lines. In our setup, we can finely adjust the free-space coupling of the light reflected from G1 and G2 to the fiber cavity, and thus the effective reflectivity of G1 and G2 provided for the  $1.1 \mu\text{m}$  and  $1.2 \mu\text{m}$  Stokes light can be independently tuned, resulting in a flexible tuning of the power ratio of the dual-wavelength RRFL. As shown in Fig. 3(a), by simultaneously rotating the angles of two gratings and tuning the pump wavelength, a dual-wavelength simultaneously tunable RRFL is realized which can emit tunable  $1.1 \mu\text{m}$  ( $1106$ – $1160$  nm) and  $1.2 \mu\text{m}$  ( $1217$ – $1280$  nm) random Raman lasing. The frequency spacing of the two

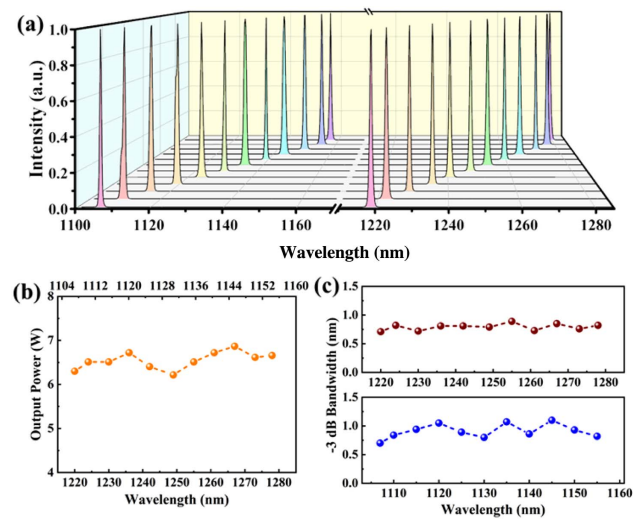


**Fig. 3.** (a) Spectra of the dual-wavelength switchable and tunable RRFL with phosphosilicate fiber under dual-wavelength operation. (b) Output powers of the dual-wavelength laser with different wavelength pairs. (c)  $-3$  dB bandwidths of the dual-wavelength laser as a function of center wavelengths.

wavelength lines is fixed at about  $26$  THz. With the fine tuning of the free-space coupling, the power ratio of the two lasing lines is equal at the maximum pump power, as verified in Fig. 3(a). The maximum output powers and  $-3$  dB bandwidths at maximum output powers of the dual-wavelength tunable RRFL for different wavelength pairs are recorded in Figs. 3(b) and 3(c), respectively. The output powers of the dual-wavelength tunable RRFL fluctuate around  $6.5$  W under  $\sim 18$  W pump power, corresponding to a conversion efficiency of  $36\%$ . The  $-3$  dB bandwidths of the two lasing lines are similar in the dual-wavelength operation mode and fluctuate in the range of  $0.65$ – $1$  nm in the whole tuning range.

### C. Separation Tunable Dual-Wavelength Emission for DFG

For the purpose of tunable DFG, the separation of the dual-wavelength laser should be tunable. This can be done in the proposed RRFL since the silica-related Raman peak has a broad Raman gain bandwidth although the phosphorus-related Raman peak is narrow, as shown in Fig. 1(b). Therefore, at a fixed pump wavelength, the emission wavelength of  $1.1 \mu\text{m}$  random lasing corresponding to the silica-related Raman peak can be tuned by tuning the reflection wavelength of G1, while the emission wavelength of  $1.2 \mu\text{m}$  random lasing is fixed at the phosphorus-related Raman peak by fixing the reflection wavelength of G2. The spectra of the wavelength separation tunable dual-wavelength RRFL are shown in Fig. 4(a); the pump wavelength is fixed at  $1064$  nm and the phosphorus-related random Raman lasing is fixed at  $1238$  nm. By tuning the reflection wavelength of G1, the silica-related random Raman lasing can be continuously tuned from  $1110$  to  $1125$  nm, and the corresponding frequency separation of the dual-wavelength RRFL can vary from  $24.3$  to  $28$  THz, which is suitable for long-wavelength tunable MIR light generation via DFG in a nonlinear crystal. The maximum output

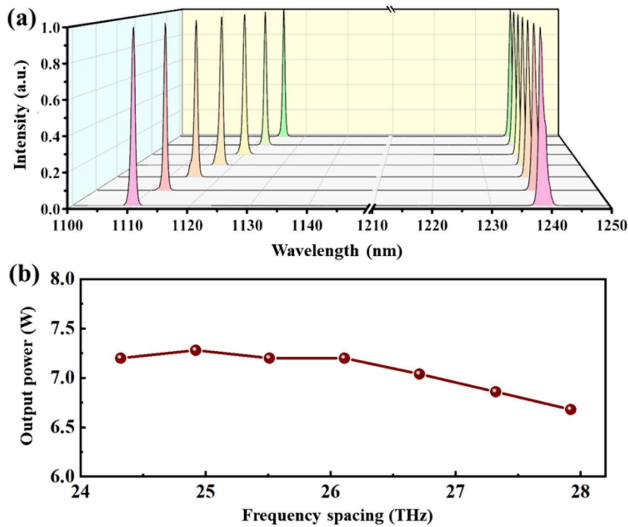


**Fig. 4.** (a) Spectra of the dual-wavelength separation tunable RRFL with phosphosilicate fiber. (b) Output powers of the dual-wavelength separation tunable RRFL with different wavelength separations.

powers of the dual-wavelength RRFL with different wavelength separations at 18 W pump power are depicted in Fig. 4(b). The output powers are around 7.2 W when the frequency separation is in the range of 24.2–26.2 THz and decrease to 6.6 W as the frequency separation increases to 28 THz. The  $-3$  dB bandwidths of the two lasing lines are around 0.8 nm.

### 3. VISIBLE LIGHT GENERATION VIA SHG AND SFG OF RRFL

Taking advantage of the broad wavelength tuning range and flexible dual-wavelength switching characteristics of the proposed RRFL based on phosphosilicate fiber, we demonstrate CW visible light with a broad wavelength tuning range by combining SHG and SFG in a PPLN crystal array. The schematic of the CW visible light generation is shown in Fig. 5(a). The RRFL is first collimated by a fiber collimator, and a long-pass filter (LPF) with a cutting-off wavelength of 1100 nm is placed after the fiber collimator to block the residual pump light. The random lasing is then focused into the PPLN crystal array through a lens with 150 mm focal length. The beam diameters at focus are estimated as  $\sim 43$   $\mu\text{m}$  and  $48$   $\mu\text{m}$  for the 1.1  $\mu\text{m}$  and 1.2  $\mu\text{m}$  wavelength components, respectively. The PPLN crystal array contains 10 separate poled gratings with quasi-phase-matching (QPM) periods ranging from 8.15 to 11.05  $\mu\text{m}$ . The dimensions of each grating are 0.5 mm (height)  $\times$  1 mm (width)  $\times$  10 mm (length). The PPLN crystal array is placed on the moving stage and the temperature of the PPLN crystal array is adjusted by a crystal oven (room temperature to 200°C) so that we can choose the specific grating period and the temperature to fulfill the QPM condition of SHG or SFG. After nonlinear frequency conversion, the residual infrared radiation is filtered by using two short-pass filters (each short-pass filter has a  $>90\%$  transmission in the range of 400–910 nm and  $<1\%$  transmission in the range of 1025–1300 nm), and the generated CW

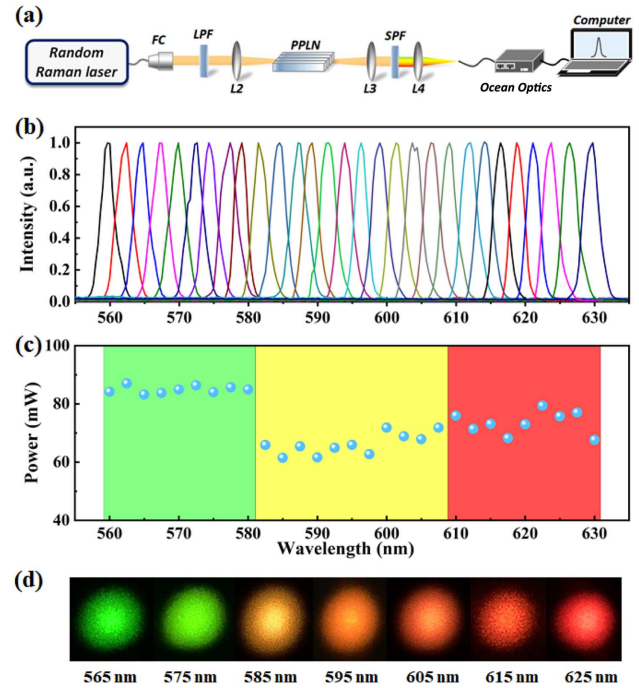


**Fig. 5.** (a) Experiment setup of the wavelength tunable CW visible light generation. (b) The experimentally measured spectra of the tunable CW visible light from 560 to 630 nm. (c) The output power of the tunable CW visible light as a function of the center wavelength. The green and red shades represent the visible components generated by the SHG of the single-wavelength tunable RRFL based on the silica-related Raman peak or phosphorus-related Raman peak, respectively, while the yellow shadow represents the visible components generated by the SFG of the dual-wavelength tunable RRFL. (d) Photograph of the wavelength tunable CW visible light with different center wavelengths.

visible light is detected by a power meter (Ophir, 3A) and a spectrometer (Ocean Optics, Maya2000).

The experimentally measured spectra of the wavelength tunable CW visible light are shown in Fig. 5(b). By combining the dual-wavelength switchable and tunable first-order RRFL with the SHG and SFG in the PPLN crystal array, CW visible light can be generated with a gap-free tuning range from 560 to 630 nm. When the RRFL operates in single-wavelength emission mode, SHG of tunable 1.1  $\mu\text{m}$  random fiber lasing (1105–1160 nm) and tunable 1.2  $\mu\text{m}$  (1217–1280 nm) random fiber lasing can be performed, respectively. The detailed phase-matching conditions for SHG are listed in Table 1. By using three grating periods as 8.15  $\mu\text{m}$ , 8.55  $\mu\text{m}$ , and 8.65  $\mu\text{m}$  and tuning the crystal temperature, SHG of 1120–1160 nm lasing can be realized and CW visible light from 560 to 580 nm can be generated. Similarly, by switching the grating periods among 10.24  $\mu\text{m}$ , 10.51  $\mu\text{m}$ , and 11.05  $\mu\text{m}$  and adjusting the temperature, SHG of 1217–1260 nm lasing can be realized, resulting in the tunable CW visible light from 608.5 to 630 nm. Meanwhile, when the RRFL operates in the dual-wavelength simultaneously tunable emission mode, SFG of the tunable 1.1  $\mu\text{m}$  and 1.2  $\mu\text{m}$  lasing lines can be performed. The phase-matching conditions of SFG are also listed in Table 1

**Table 1. Phase-Matching Conditions in PPLN Crystal Array**

	QPM Period ( $\mu\text{m}$ )	Temperature ( $^{\circ}\text{C}$ )	Output Wavelength (nm)
SHG	8.15	45–200	560–569
	8.55	47–200	569–578
	8.65	157–190	578–580
SFG	9.05	52–180	580–587.5
	9.45	30–200	587.5–597.5
	9.70	110–190	597.5–602.5
	9.97	100–190	602.5–608.5
SHG	10.24	100–180	608.5–612.5
	10.51	80–200	612.5–620
	11.05	30–190	620–630

with the use of four different grating periods and the temperature tuning. As a result, 580–608.5 nm tunable visible CW light can be generated via SFG. Therefore, as depicted in Fig. 5(b), gap-free continuous tuning of CW visible light in the range of 560–630 nm is experimentally demonstrated via SHG and SFG of the proposed RRFL, which is the widest tuning range of visible light generated from an RFL. Due to the relatively low spectral resolution of the spectrometer (Ocean Optics, Maya2000) used in our experiment, the bandwidth of CW visible light cannot be measured accurately. It should be noted that with more suitable PPLN grating periods, it is feasible to realize CW visible light with a wavelength tuning range over 85 nm (552.5–640 nm) based on the wavelength tuning range of the RRFL.

The maximum output powers of the wavelength tunable CW visible light at different center wavelengths are plotted in Fig. 5(c). Green and red shades represent the visible components generated by the SHG of the single-wavelength tunable random lasing based on the silica-related Raman peak or phosphorus-related Raman peak, respectively. The yellow shadow represents the visible components generated by the SFG of the dual-wavelength tunable random lasing. The output power of SHG of tunable 1.1  $\mu\text{m}$  random fiber lasing is about 85 mW under the maximum power of the fundamental light (in the range of 6.1–7.3 W). Meanwhile, the output powers of SFG and SHG of tunable 1.2  $\mu\text{m}$  random fiber lasing fluctuate around 65 mW and 70 mW, respectively. It is worth mentioning that the generated random Raman lasing is non-polarized, and thus only one half of the power with certain linearly polarized component is effectively involved in the SHG or SFG in the PPLN crystal. Further power scaling of the tunable visible light can be done by using a more powerful RRFL [12–15] and the linearly polarized RRFL [42]. The linearly polarized RRFL is beneficial for enhancing efficiency of SHG or SFG in the PPLN crystal. However, for the DFG process in BGSe crystal with Type I phase matching, the polarization of the pump and signal light should be different; therefore, the linearly polarized dual-wavelength RRFL cannot be used for the DFG process present in the next section. Figure 5(d) is the photograph of the bright emission of the wavelength tunable CW visible light with the colors across multiple color regions including green, yellow, orange, and red. The generated broadly tunable visible light with decent output power has great

potential for applications in speckle-free imaging, wavelength selective illumination [43], hyperspectral imaging and sensing [44], and visible temporal ghost imaging.

#### 4. MIR LIGHT GENERATION VIA DFG OF RRFL

The experiment setup of the CW DFG based on the proposed RRFL operating in the separation tunable dual-wavelength emission mode is shown in Fig. 6(a). The RRFL is first collimated with a fiber collimator and an LPF is used to filter out the residual pump component. A mechanical chopper is placed at the beam path with a chopping frequency of 1 kHz. Then the laser beam is focused with a lens of 175 mm focal length into the BGSe crystal. The beam diameters at focus are estimated as  $\sim 50 \mu\text{m}$  and  $56 \mu\text{m}$  for the 1.1  $\mu\text{m}$  and 1.2  $\mu\text{m}$  wavelength components, respectively. The BGSe crystal (supplied by Technical Institute of Physics and Chemistry, Chinese Academy of Sciences) has an aperture of 5 mm  $\times$  7 mm and a length of 10 mm, with the AR coatings at 1–1.5  $\mu\text{m}$  and 10–14  $\mu\text{m}$ . The transmission spectrum of the coated BGSe crystal is shown in the inset of Fig. 6(a). The BGSe crystal is cut at  $\theta = 47^{\circ}$  and  $\varphi = 0^{\circ}$  for Type I (e-e-o) phase matching and is mounted on a rotation stage so that the spectral tuning can be realized by rotating the phase-matching angle of the nonlinear crystal. Since the used RRFL is nonpolarized, the specific linearly polarized components of 1.1  $\mu\text{m}$  and 1.2  $\mu\text{m}$  lasing are effectively involved in DFG. The generated CW MIR light after the crystal is first collimated by an uncoated ZnSe lens with a 100 mm focal length and then passes through an AR-coated germanium filter which is used to block the residual dual-wavelength random fiber lasing. For the spectral measurement, the MIR light is focused by a ZnSe lens

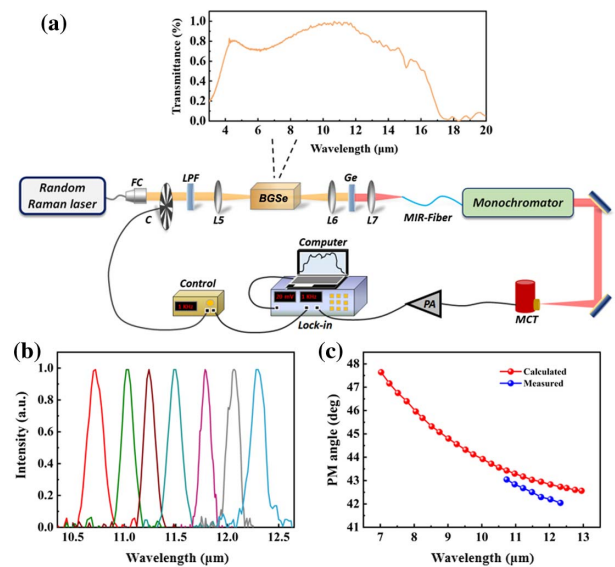


**Fig. 6.** (a) Experimental setup of the wavelength tunable CW MIR light generation. Inset: transmission spectrum of coated BGSe crystal. (b) The experimentally measured spectra of the CW MIR light from 10.7 to 12.3  $\mu\text{m}$ . (c) The calculated (red) and measured (blue) Type I (e-e-o) phase-matching curves of BGSe with a fixed signal wavelength of 1238 nm. Ge, germanium filter; C, chopper; MCT, HgCdTe detector; PA, preamplifier.

(3–12  $\mu\text{m}$  AR-coated) with a 50 mm focal length into a hollow-core MIR fiber (OptoKnowledge HF500MW), and then detected by a grating-scanning monochromator (Zolix Omni- $\lambda$ 500i) with a liquid nitrogen cooled HgCdTe detector (Judson, DMCT16-De01). To measure the MIR output power, the MIR radiation is directly focused onto the HgCdTe detector. The output electrical signal of the detector is amplified by a low-noise preamplifier, and then fed into a lock-in amplifier for optical power demodulation.

In the dual-wavelength separation tunable RRFL, the laser line which can be tuned from 1110 to 1125 nm acts as the pump in DFG and the laser line at 1238 nm is the signal in DFG. Figure 6(b) shows the experimentally measured spectra of the tunable CW MIR light by simultaneously tuning the pump wavelength and the angle of the BGSe crystal. As a result, continuous wavelength tuning of the MIR idler wave from 10.7 to 12.3  $\mu\text{m}$  could be realized corresponding to the frequency spacing from 24.3 to 28 THz for the dual-wavelength separation tunable RRFL. The  $-3$  dB bandwidths of the generated CW MIR light fluctuate around 120 nm. Figure 6(c) depicts the Type I phase-matching angle curves of the BGSe crystal calculated by Sellmeier equations reported in Ref. [45] with a fixed signal wavelength of 1238 nm and experimentally measured data, respectively. In our experiment, the phase-matching angle is measured from  $43.1^\circ$  to  $42.1^\circ$  to fulfill the phase-matching condition for generating MIR idler wave in the range of 10.7 to 12.3  $\mu\text{m}$ . The discrepancy between the measured and calculated phase-matching curves of BGSe in the long-wavelength MIR region has also been reported in Ref. [46]. We also measured the output powers of the MIR DFG radiations at different center wavelengths. Optical losses caused by the germanium filter, ZnSe lens, and the MCT detector are corrected. The highest CW MIR light output power of  $7.2 \mu\text{W}$  is obtained at the center wavelength of 10.7  $\mu\text{m}$  under an RRFL output power of 6.6 W, while the output powers of the MIR idler wave with longer wavelength are decreased to  $6.5 \mu\text{W}$ ,  $4.8 \mu\text{W}$ ,  $4.3 \mu\text{W}$ , and  $3.5 \mu\text{W}$  at 11  $\mu\text{m}$ , 11.5  $\mu\text{m}$ , 11.75  $\mu\text{m}$ , and 12.3  $\mu\text{m}$ , respectively. Although the conversion efficiency of CW DFG is relatively low, the power of the MIR light is enough for spectroscopic applications [47–49].

In previous demonstrations of CW DFG beyond 10  $\mu\text{m}$ , AgGaS<sub>2</sub>/Se<sub>2</sub> [47], LiInS<sub>2</sub> [48], and GaSe [49] are used as nonlinear crystals and the DFG is driven by two laser sources including gas lasers, solid-state Ti:sapphire lasers, and diode lasers [47–50]. AgGaS<sub>2</sub> has a moderate transparent spectral range up to 12  $\mu\text{m}$  and AgGaSe<sub>2</sub> has a low damage threshold caused by a small bandgap energy of 1.8 eV. LiInS<sub>2</sub> is limited by the spectral transmission range up to 11  $\mu\text{m}$  and a relatively small nonlinear coefficient. GaSe has a broad transmission range up to 18  $\mu\text{m}$ ; however, it could be cleaved only along the (001) plane ( $z$ -cut,  $\theta = 0^\circ$ ) and cannot be anti-reflection coated. We realize the first experimental demonstration of CW DFG beyond 10  $\mu\text{m}$  based on the BGSe crystal featuring a broad transparency range spanning from 0.47 to 18  $\mu\text{m}$ , decent nonlinearity, and relatively high damage threshold, and the achieved power of the  $>10 \mu\text{m}$  MIR idler wave already exceeds the previously reported ones [47–50]. Since there is no sign of power saturation and crystal damage, further power scaling

of the  $>10 \mu\text{m}$  DFG source based on BGSe crystal is promising with a more powerful RRFL. Moreover, compared to the use of two laser sources in DFG, the use of a single fiber laser with dual-wavelength separation tunable emission can lead to a simple, compact, and robust DFG source. Therefore, we believe the combination of the proposed dual-wavelength separation tunable RRFL and new nonlinear crystal BGSe can provide a promising platform for generating tunable CW MIR light in the  $>10 \mu\text{m}$  long wavelength region, which can have important applications in spectroscopy and imaging.

## 5. DISCUSSION AND PROSPECTS

In our proposed RRFL, free-space optics components are used to form the point feedback unit. It is worth mentioning that it is also feasible to realize a dual-wavelength switchable and tunable RRFL with an all-fiber structure, which can be more compact and robust. Figure 7 shows the schematic diagram of a dual-wavelength switchable and tunable RRFL with all-fiber structure. A specially designed WDM is used to separate the two Stokes wavelengths in the point feedback unit. Since the gain bandwidth of the phosphorus-related Raman peak is narrow, a fiber loop mirror is connected to the 1.2–1.3  $\mu\text{m}$  port of the WDM so that the random lasing wavelength corresponding to the phosphorus-related Raman peak is determined by the pump wavelength and can be tuned by tuning the pump wavelength. On the contrary, to realize the dual-wavelength separation tunable RRFL, a tunable optical filter such as an acousto-optic tunable filter [51] is inserted in the fiber loop mirror connected to the 1.1–1.16  $\mu\text{m}$  port of the WDM to realize wavelength tuning of random lasing corresponding to the broad silica-related Raman peak at a fixed pump wavelength. Two variable optical attenuators are used in the point feedback unit to adjust the feedback strength for the two Stokes wavelengths to realize dual-wavelength switchable operation [37].

It should be also noted that there is another relatively broad boson peak located around 3.65 THz in the Raman gain spectrum of the phosphosilicate fiber shown in Fig. 1(b). Such a boson peak has been used to generate ultralow quantum defect Raman lasing [17,52] and can potentially be used to generate tunable Raman lasing. It is expected that tunable MIR source around 8.25  $\mu\text{m}$  can be realized by using DFG of dual-wavelength lasing corresponding to the boson peak and phosphorus-related peak. More colors in visible can also be generated by utilizing the boson peak related lasing in SHG and SFG processes.

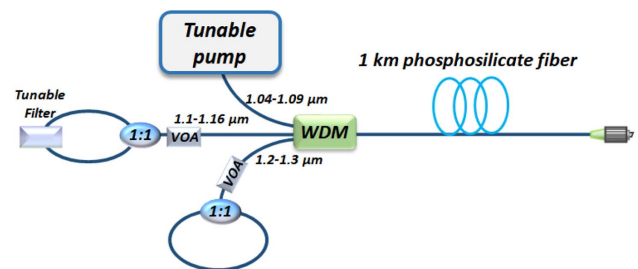


**Fig. 7.** Schematic diagram of dual-wavelength switchable and tunable RRFL with all-fiber structure. WDM, wavelength-division multiplexer; VOA, variable optical attenuator.

## 6. CONCLUSION

In conclusion, a dual-wavelength switchable and tunable RRFL based on phosphosilicate fiber is developed for the first time, and the spectrum of the proposed RRFL can be flexibly manipulated to meet the requirements of different nonlinear frequency conversion processes, including single-wavelength tunable emission at the 1.1  $\mu\text{m}$  or 1.2  $\mu\text{m}$  band for SHG, dual-wavelength simultaneously tunable emission at the 1.1  $\mu\text{m}$  and 1.2  $\mu\text{m}$  bands for the SFG, and separation tunable dual-wavelength emission for DFG. Benefiting from the spectra flexible characteristic, the superior capability of the proposed RRFL to generate widely tunable CW visible and mid-infrared light via nonlinear frequency conversions is experimentally demonstrated. As a result, by combining SHG and SFG in a PPLN crystal array, tunable CW visible light with a record tuning range (560–630 nm) generated from the RFL can be realized. CW MIR light with a wavelength tuning range from 10.7 to 12.3  $\mu\text{m}$  is also demonstrated via DFG of the proposed RRFL in a BGSe crystal. Our experimental results show that the developed dual-wavelength switchable and tunable RRFL can provide a compact, robust, and cost-effective platform for performing multifunctional nonlinear frequency conversion processes and generating widely tunable light in both the visible and MIR regions, which can potentially extend the applications of RFLs such as imaging and sensing in various spectral regions.

**Funding.** National Natural Science Foundation of China (62005186, 62075144, 61875132); Engineering Featured Team Fund of Sichuan University (2020SCUNG105); Fundamental Research Funds for the Central Universities (YJ201979, YJ201982).

**Disclosures.** The authors declare no conflicts of interest.

**Data Availability.** Data underlying the results presented in this paper are not publicly available at this time but may be obtained from the authors upon reasonable request.

## REFERENCES

- S. K. Turitsyn, S. A. Babin, A. E. El-Taher, P. Harper, D. V. Churkin, S. I. Kablukov, J. D. Ania-Castañón, V. Karalekas, and E. V. Podivilov, "Random distributed feedback fibre laser," *Nat. Photonics* **4**, 231–235 (2010).
- D. V. Churkin, S. Sugavanam, I. D. Vatik, Z. Wang, E. Podivilov, S. A. Babin, Y. Rao, and S. K. Turitsyn, "Recent advances in fundamentals and applications of random fiber lasers," *Adv. Opt. Photonics* **7**, 516–569 (2015).
- A. S. L. Gomes, A. L. Moura, C. B. de Araújo, and E. P. Raposo, "Recent advances and applications of random lasers and random fiber lasers," *Prog. Quantum Electron.* **78**, 100343 (2021).
- Z. N. Wang, H. Wu, M. Q. Fan, L. Zhang, Y. J. Rao, W. L. Zhang, and X. H. Jia, "High power random fiber laser with short cavity length: theoretical and experimental investigations," *IEEE J. Sel. Top. Quantum Electron.* **21**, 0900506 (2015).
- I. D. Vatik, D. V. Churkin, E. V. Podivilov, and S. A. Babin, "High-efficiency generation in a short random fiber laser," *Laser Phys. Lett.* **11**, 075101 (2014).
- J. X. Song, S. Ren, W. Liu, W. Li, H. Wu, P. Ma, H. S. Zhang, and P. Zhou, "Temporally stable fiber amplifier pumped random distributed feedback Raman fiber laser with record output power," *Opt. Lett.* **46**, 5031–5034 (2021).
- J. Ye, J. M. Xu, J. X. Song, H. S. Wu, H. W. Zhang, J. Wu, and P. Zhou, "Flexible spectral manipulation property of a high power linearly polarized random fiber laser," *Sci. Rep.* **8**, 2173 (2018).
- H. Wu, Z. Wang, M. Fan, L. Zhang, W. Zhang, and Y. Rao, "Role of the mirror's reflectivity in forward-pumped random fiber laser," *Opt. Express* **23**, 1421–1427 (2015).
- S. A. Babin, A. E. El-Taher, P. Harper, E. V. Podivilov, and S. K. Turitsyn, "Tunable random fiber laser," *Phys. Rev. A* **84**, 021805 (2011).
- A. E. El-Taher, P. Harper, S. A. Babin, D. V. Churkin, E. V. Podivilov, J. D. Ania-Castañón, and S. K. Turitsyn, "Effect of Rayleigh-scattering distributed feedback on multi-wavelength Raman fiber laser generation," *Opt. Lett.* **36**, 130–132 (2011).
- M. Shen, J. Deng, Y. Li, and X. Shu, "Multi-wavelength random fiber laser based on a tilted parallel inscribed apodized fiber Bragg grating array," *Opt. Lett.* **47**, 5473–5476 (2022).
- L. Zhang, H. Jiang, X. Yang, W. Pan, S. Cui, and Y. Feng, "Nearly-octave wavelength tuning of a continuous wave fiber laser," *Sci. Rep.* **7**, 42611 (2017).
- J. Y. Dong, L. Zhang, H. W. Jiang, X. Z. Yang, W. W. Pan, S. Z. Cui, and Y. Feng, "High order cascaded Raman random fiber laser with high spectral purity," *Opt. Express* **26**, 5275–5280 (2018).
- V. Balaswamy, S. Aparanji, S. Arun, S. Ramachandran, and V. R. Supradeepa, "High-power, widely wavelength tunable, grating free Raman fiber laser based on filtered feedback," *Opt. Lett.* **44**, 279–282 (2019).
- V. Balaswamy, S. Ramachandran, and V. R. Supradeepa, "High-power, cascaded random Raman fiber laser with near complete conversion over wide wavelength and power tuning," *Opt. Express* **27**, 9725–9732 (2019).
- B. Han, Y. Rao, H. Wu, J. Yao, H. Guan, R. Ma, and Z. Wang, "Low-noise high-order Raman fiber laser pumped by random lasing," *Opt. Lett.* **45**, 5804–5807 (2020).
- Y. Zhang, S. Li, J. Ye, X. Ma, J. Xu, T. Yao, and P. Zhou, "Low quantum defect random Raman fiber laser," *Opt. Lett.* **47**, 1109–1112 (2022).
- H. Wu, B. Han, Z. Wang, G. Genty, G. Feng, and H. Liang, "Temporal ghost imaging with random fiber lasers," *Opt. Express* **28**, 9957–9964 (2020).
- D. Xiang, P. Lu, Y. Xu, S. Gao, L. Chen, and X. Bao, "Truly random bit generation based on a novel random Brillouin fiber laser," *Opt. Lett.* **40**, 5415–5418 (2015).
- F. Monet, J. S. Boisvert, and R. Kashyap, "A simple high-speed random number generator with minimal post-processing using a random Raman fiber laser," *Sci. Rep.* **11**, 13182 (2021).
- H. Wu, J. Xiong, B. Han, Z. N. Wang, W. L. Zhang, X. H. Jia, and H. K. Liang, "Ultra-high speed random bit generation based on Rayleigh feedback assisted ytterbium-doped random fiber laser," *Sci. China Technol. Sci.* **64**, 1295–1301 (2021).
- R. Ma, Y. J. Rao, W. L. Zhang, and B. Hu, "Multi-mode random fiber laser for speckle-free imaging," *IEEE J. Sel. Top. Quantum Electron.* **25**, 0900106 (2019).
- J. Lv, H. Li, Y. Zhang, L. Deng, X. Ma, C. Gu, P. Yao, L. Xu, and Q. Zhan, "Tailoring the spectrum and spatial mode of Yb-doped random fiber laser," *Opt. Express* **30**, 8345–8355 (2022).
- X. Y. Ma, J. Ye, Y. Zhang, J. M. Xu, J. Wu, T. F. Yao, J. Y. Leng, and P. Zhou, "Vortex random fiber laser with controllable orbital angular momentum mode," *Photonics Res.* **9**, 266–271 (2021).
- R. Ma, Z. Wang, H. Zhang, W. Zhang, and Y. Rao, "Imaging through opacity using a near-infrared low-spatial coherence fiber light source," *Opt. Lett.* **45**, 3816–3819 (2020).
- F. Y. Lin and J. M. Liu, "Chaotic lidar," *IEEE J. Sel. Top. Quantum Electron.* **10**, 991–997 (2004).
- E. I. Dontsova, S. I. Kablukov, I. D. Vatik, and S. A. Babin, "Frequency doubling of Raman fiber lasers with random distributed feedback," *Opt. Lett.* **41**, 1439–1442 (2016).
- S. Rota-Rodrigo, B. Gouhier, C. Dixneuf, L. Antoni-Micollier, G. Guiraud, D. Leandro, M. Lopez-Amo, N. Traynor, and G. Santarelli,

- "Watt-level green random laser at 532 nm by SHG of a Yb-doped fiber laser," *Opt. Lett.* **43**, 4284–4287 (2018).
29. S. Cui, J. Qian, X. Zeng, X. Cheng, X. Gu, and Y. Feng, "A watt-level yellow random laser via single-pass frequency doubling of a random Raman fiber laser," *Opt. Fiber Technol.* **64**, 102552 (2021).
  30. H. Wu, H. Liu, W. Wang, Z. Wang, and H. Liang, "Tailoring the efficiency and spectrum of a green random laser generated by frequency doubling of random fiber lasers," *Opt. Express* **29**, 21521–21529 (2021).
  31. H. Wu, W. Wang, B. Hu, R. Ma, J. Liu, and H. Liang, "Multi-color switchable visible light source generated via nonlinear frequency conversion of a random fiber laser," *Opt. Express* **30**, 44785–44797 (2022).
  32. B. Hu, H. Wu, K. Tian, and H. Liang, "Continuous-wave 2.9–3.8  $\mu\text{m}$  random lasing via temperature-tuning free difference-frequency generation of random fiber lasers in PPLN crystal," *Sci. China Inf. Sci.* **66**, 189401 (2023).
  33. J. Yao, W. Yin, K. Feng, X. Li, D. Mei, Q. Lu, Y. Ni, Z. Zhang, Z. Hu, and Y. Wu, "Growth and characterization of  $\text{BaGa}_4\text{Se}_7$  crystal," *J. Cryst. Growth* **346**, 1–4 (2012).
  34. J. Zhang, Q. Wang, J. Hao, H. Liu, J. Yao, Z. Li, J. Liu, and K. F. Mak, "Broadband, few-cycle mid-infrared continuum based on the intrapulse difference frequency generation with BGSe crystals," *Opt. Express* **28**, 37903–37909 (2020).
  35. H. Wu, W. Wang, Y. Li, C. Li, J. Yao, Z. Wang, and H. Liang, "Difference-frequency generation of random fiber lasers for broadly tunable mid-infrared continuous-wave random lasing generation," *J. Lightwave Technol.* **40**, 2965–2970 (2022).
  36. M. Sun, Z. Cao, J. Yao, H. Ma, Y. Guo, X. Gao, R. Rao, and Y. Wu, "Continuous-wave difference-frequency generation based on  $\text{BaGa}_4\text{Se}_7$  crystal," *Opt. Express* **27**, 4014–4023 (2019).
  37. J. Song, J. Xu, Y. Zhang, J. Ye, and P. Zhou, "Phosphosilicate fiber based dual-wavelength random fiber laser with flexible power proportion and high spectral purity," *Opt. Express* **27**, 23095–23102 (2019).
  38. D. Y. Liu, B. Huang, L. L. Yang, J. D. Wu, N. Li, L. L. Miao, and C. J. Zhao, "Widely tunable narrow linewidth dual-wavelength Yb-doped fiber laser with inhomogeneous polarization output," *J. Lightwave Technol.* **41**, 327–332 (2023).
  39. H. Wu, B. Han, and Y. Liu, "Tunable narrowband cascaded random Raman fiber laser," *Opt. Express* **29**, 21539–21550 (2021).
  40. A. R. Sarmani, M. H. A. Bakar, A. A. A. Bakar, F. R. M. Adikan, and M. A. Mahdi, "Spectral variations of the output spectrum in a random distributed feedback Raman fiber laser," *Opt. Express* **19**, 14152–14159 (2011).
  41. J. Xu, J. Ye, W. Liu, J. Wu, H. Zhang, J. Leng, and P. Zhou, "Passively spatiotemporal gain-modulation-induced stable pulsing operation of a random fiber laser," *Photonics Res.* **5**, 598–603 (2017).
  42. E. A. Zlobina, S. I. Kablukov, and S. A. Babin, "Linearly polarized random fiber laser with ultimate efficiency," *Opt. Lett.* **40**, 4074–4077 (2015).
  43. R. Ma, Z. Wang, W. Y. Wang, Y. Zhang, J. Liu, W. L. Zhang, A. S. L. Gomes, and D. Y. Fan, "Wavelength-dependent speckle multiplexing for imaging through opacity," *Opt. Laser Eng.* **141**, 106567 (2021).
  44. K. Monakhova, K. Yanny, N. Aggarwal, and L. Waller, "Spectral DiffuserCam: lensless snapshot hyperspectral imaging with a spectral filter array," *Optica* **7**, 1298–1307 (2020).
  45. E. Boursier, P. Segonds, B. Ménaert, V. Badikov, V. Panyutin, D. Badikov, V. Petrov, and B. Boulanger, "Phase-matching directions and refined Sellmeier equations of the monoclinic acentric crystal  $\text{BaGa}_4\text{Se}_7$ ," *Opt. Lett.* **41**, 2731–2734 (2016).
  46. K. Tian, W. Z. Wang, C. X. Li, Z. J. Wan, B. Hu, L. Z. He, M. X. Xiang, J. Y. Yao, H. Wu, and H. K. Liang, "Ultrabroad (3.7–17  $\mu\text{m}$ ) tunable femtosecond optical parametric amplifier based on  $\text{BaGa}_4\text{Se}_7$  crystal," *Opt. Lett.* **47**, 5973–5976 (2022).
  47. U. Simon, C. E. Miller, C. C. Bradley, R. G. Hulet, R. F. Curl, and F. K. Tittel, "Difference-frequency generation in  $\text{AgGaS}_2$  by use of single-mode diode-laser pump sources," *Opt. Lett.* **18**, 1062–1064 (1993).
  48. S. Fossier, S. Salaün, J. Mangin, O. Bidault, I. Thénot, J. J. Zondy, W. Chen, F. Rotermund, V. Petrov, P. Petrov, J. Henningsen, A. Yelissev, L. Isaenko, S. Lobanov, O. Balachninaite, G. Sleky, and V. Sirutkaitis, "Optical, vibrational, thermal, electrical, damage, and phase-matching properties of lithium thioindate," *J. Opt. Soc. Am. B* **21**, 1981–2007 (2004).
  49. W. Chen, F. Cazier, F. Tittel, and D. Boucher, "Measurements of benzene concentration by difference-frequency laser absorption spectroscopy," *Appl. Opt.* **39**, 6238–6242 (2000).
  50. V. Petrov, "Frequency down-conversion of solid-state laser sources to the mid-infrared spectral range using non-oxide nonlinear crystals," *Prog. Quantum Electron.* **42**, 1–106 (2015).
  51. S. Li, J. Xu, J. Liang, J. Ye, Y. Zhang, X. Ma, J. Leng, and P. Zhou, "Multi-wavelength random fiber laser with a spectral-flexible characteristic," *Photonics Res.* **11**, 159–164 (2023).
  52. X. Ma, J. Xu, J. Ye, Y. Zhang, L. Huang, T. Yao, J. Leng, Z. Pan, and P. Zhou, "Cladding-pumped Raman fiber laser with 0.78% quantum defect enabled by phosphorus-doped fiber," *High Power Laser Sci. Eng.* **10**, e8 (2022).